Facies (2011) 57:605–612
DOI 10.1007/s10347-010-0257-6

ORIGINAL ARTICLE

TEM study of Mg distribution in micrite crystals from the Mishrif reservoir Formation (Middle East, Cenomanian to Early Turonian)

Chadia Volery · Elena Suvorova · Philippe Buffat · Eric Davaud · Bruno Caline

Received: 18 February 2010 / Accepted: 23 December 2010 / Published online: 30 January 2011

Abstract Microporous limestones composed of micrite crystals constitute sizeable hydrocarbon reservoirs throughout the world and especially in the Middle East. However, the crystallization history of micrites is poorly understood. Scanning electronic microscopy (SEM) with X-ray energy dispersive spectroscopy (EDS) studies give morphological and bulk composition information about micrites, but no information exists on the distribution of minor elements inside micrite grains. This study proposes Mg maps obtained with X-ray EDS combined with scanning transmission electron microscopy (STEM) of micrite crystals from the Mishrif reservoir Formation (Middle East, Cenomanian to Early Turonian). Three types of Mg distribution were observed through micrite crystals from five different samples: (1) homogenous Mg concentration, (2) small Mg-enriched areas close to the center of the crystal, and (3) geometric Mg impoverishments near crystal edges and parallel to present crystallographic faces. The homogenous Mg distribution is the most frequent and is found both in microporous and in tight micrites. The second type of distribution showing small Mg-enriched areas inside micrite crystals relatively close to their center comes from a microporous sample located below an emersive surface. These enriched areas may correspond to crystal seeds. The third type of distribution was observed in micrite crystals from another microporous sample situated just below an emersive surface. The Mg-poor zones probably represent overgrowths that precipitated in contact with less Mg-rich meteoric fluids.

Keywords Micrite · Microporosity · TEM · Mg · Mishrif

C. Volery · E. Davaud
Department of Geology and Palaeontology,
Earth and Environmental Sciences, University of Geneva,
Rue des Maraîchers 13, 1205 Geneva, Switzerland

E. Davaud
e-mail: Eric.Davaud@unige.ch

C. Volery (✉)
Shell International Exploration and Production,
Kessler Park 1, 2288 GS Rijswijk, The Netherlands
e-mail: Chadia.Volery@shell.com; chadia@infomaniak.ch

E. Suvorova · P. Buffat
Centre Interdisciplinaire de Microscopie Electronique,
Ecole Polytechnique Fédérale de Lausanne, MXC,
Station 12, 1015 Lausanne, Switzerland
e-mail: elena.suvorova@epfl.ch

P. Buffat
e-mail: philippe.buffat@epfl.ch

B. Caline
Total Exploration and Production, CSTJF,
Avenue Larribau, 64000 Pau, France
e-mail: bruno.caline@total.com

Introduction

Micritic limestones are dominantly constituted by low-Mg calcite crystals with sub-rhombic shape and size generally below 4 μm according to Folk's (1959) definition. Some of these micritic limestones are microporous and are of considerable economic interest as petroleum reservoirs, especially in the Middle East. Because of their smallness, micrite crystals remained unidentified for a long time. With the development of the SEM, numerous features have been discovered. In the 1970s, Loreau (1972) presented the first morphological classification of micrites. However, the formation of these microporous limestones is still a matter of debate: there are nearly as many hypotheses about their origin as there are authors of articles (Ahr 1989; Budd

1989; Cantrell and Hagerty 1999; Kaldi 1989; Lambert et al. 2006; Moshier 1989; Perkins 1989; Richard et al. 2007; Saller and Moore 1989). Scientists agree on the final low-Mg calcite nature of the micro-rhombohedra, but the mineralogy of the precursor carbonate mud (aragonitic or calcitic) and the role played by the diagenetic processes remain unclearly identified. Recently, the importance of a precursor mud mainly composed of low-Mg calcite crystals and of early meteoric processes to form and preserve the microporosity in micritic limestones was demonstrated (Volery et al. 2009, 2010a, b). The micrite crystals and the associated microporous network are thought to be primary features, partly conserved during moderate diagenesis. These new results may be confirmed by highly precise chemical analyses of micrite crystals.

Cathodoluminescence microscopy is very useful to decrypt diagenetic processes involved in the formation of limestones. Unfortunately, such technology cannot provide information about the mineralogical composition evolution of micrite crystals, because of their smallness. However, in order to better understand the history of micrites and to determine if these crystals generally result from a unique phase of (re)crystallization or rather several phases of (re)crystallization, these data are primordial.

Nowadays, no information exists on the distribution of minor elements inside a single micrite grain. Mg is the main element incorporated in calcite, but it often represents only a few mol% $MgCO_3$. Scanning electron microscopy (SEM) with X-ray energy dispersive spectroscopy (EDS) is generally not adapted to quantify such minor Mg concentration variations in very fine crystals. However, ultra-thin sections analyzed with X-ray EDS combined with the scanning transmission electron microscopy (STEM) allow fine variations of minor elements inside small crystals to be highlighted.

Several TEM studies have already explored the nanometric structures of synthetic calcite crystals (Chien et al. 2006; Paquette et al. 1996, 1999) and the early nucleation of calcium carbonate (Pouget et al. 2009), but no work was done on the distribution of minor elements inside a single micrite grain of ancient rocks. Using samples from a typical micritic reservoir, the Mishrif Formation (Cenomanian to Early Turonian, Middle East), this study proposes several maps of the Mg distribution inside micrite crystals obtained with X-ray EDS combined with STEM.

Geological setting

The Cretaceous of the Middle East is composed of three major shallowing-upwards sedimentological cycles separated by unconformities (Alsharhan and Nairn 1993; Haq and Al-Qahtani 2005; Harris et al. 1984; Sharland et al. 2001): the Thamama Group (Early Tithonian to Late Aptian), the Wasia Group (Early Albian to Early Turonian) and the Aruma Group (Late Turonian to Early Danian). The Mishrif reservoir Formation (Cenomanian to Early Turonian) represents the last deposits of the Wasia Group and consists of shallow-marine carbonates with rudist bioherms (Alsharhan and Nairn 1993; Harris et al. 1984). It settled on carbonate ramps and low-gradient shelves rimming intra-shelf basins (Aqrawi et al. 1998; Burchette 1993; Philip et al. 1995) during sea-level highstand (Haq and Al-Qahtani 2005) and calcite seas period (Dickson 2002; Hardie 1996; Lowenstein et al. 2001; Sandberg 1983). In the Mesopotamian basin, the lateral extension of the Mishrif Formation reaches more than 900 km (Reulet 1977) and its thickness attains about 400 m in southeastern Iraq (Aqrawi et al. 1998).

The Mishrif Formation in the Mesopotamian basin is composed of two major shallowing-upwards sequences (Aqrawi et al. 1998; Reulet 1977). Samples analyzed in this study come from Qatar (depth: 1,405 m) and Iraq (depths: 3,816, 3,829, 3,878, and 3,897 m) from the second (the youngest) shallowing-upwards sequence. The four samples from Iraq were chosen in two distinctive wells (well X: 3,816 and 3,829 m; well Y: 3,878 and 3,897 m). Sample 1,405 m in Qatar is a wackestone dominated by large foraminifera, rudists, bivalves, and echinoderms. It may correspond to a lagoonal deposit. In Iraq, sample 3,816 m is a wackestone to packstone with rudists, bivalves and small foraminifera; sample 3,829 m is characterized by a floatstone made of large rudist debris, bivalves, and echinoderms; sample 3,878 m is a wackestone with rudists, bivalves, echinoderms and small foraminifera; sample 3,897 m consists in a wackestone to packstone with rudists, bivalves and echinoderms. All samples of Iraq probably represent internal platform deposits, with slight differences of energy level. Particularly, sample 3,829 m may be located near a rudists-rich shoal.

During the Early Turonian, the Mishrif Formation underwent erosion and meteoric diagenesis principally linked to a major sea-level fall (Alsharhan and Nairn 1993; Haq and Al-Qahtani 2005; Harris et al. 1984). Samples 3,829, 3,897, and 1,405 m are each situated few meters below a different emersive surface (distances to the emersive surface, respectively: $\sim$3, $\sim$13, and $\sim$25 m) (unpublished Total report 2009). Transgressive conditions returned during the Late Turonian deposing the Khasib Formation (Aqrawi et al. 1998; Cavazza et al. 2004; Sharland et al. 2001; Ziegler 2001) that sealed the Mishrif reservoir rocks.

Methods

Petrophysical, mineralogical, and chemical analyses

Analyses were performed in Total laboratories. The porosity (phi) of samples was measured with helium. The

permeability (K) was calculated with nitrogen and corrected for the Klinkenberg effect. The mineralogical and chemical composition was identified by X-ray diffraction (XRD) and X-ray fluorescence (XRF) analyses. Diffraction peaks were measured for angles from 4.5 to 70°. The XRD device was an XPert Pro manufactured by PANalytical and the XRF device a Pioneer S4 manufactured by Bruker.

Electron microscopy study

Electron microscopy studies were conducted in the Ecole Polytechnique Fédérale, Lausanne (EPFL). In a first stage, polished and carbon-coated samples were studied in a FEI XL30 SFEG scanning electron microscope (SEM) at 3–5 kV accelerating voltage. Local analyses to investigate the distribution of the Mg element in micrite crystals was performed by transmission electron microscopy (TEM), scanning transmission electron microscopy (STEM), and X-ray energy dispersive spectroscopy (EDS) in a FEI CM 300FEG-UT analytical transmission electron microscope (300-kV field emission gun, 20° X-ray take-off angle). For TEM, STEM, and X-ray EDS examination, slices about 100 nm thick were cut by ultramicrotomy at room temperature with a diamond knife after epoxy embedding and solidifying for 2 days. These slices were collected in demineralized water with a drop of ethanol and mounted on a copper ring. The effect of charging up was suppressed by 5–15 nm carbon coating of samples.

The TEM images and electron diffraction patterns were recorded with a Gatan 797 slow scan CCD camera (1,024 pixels × 1,024 pixels × 14 bits) and processed with the Gatan Digital Micrograph 3.11.0 software. The distribution of Mg over a particular micrite single crystal was viewed using element maps in STEM mode and interpreted with the Oxford INCA software. Quantification was performed with the QuantMap software application designed to generate quantitative elemental maps from SmartMap data. The quantitative data are calculated from spectral data stored at each pixel of the SmartMap. The thickness effect (thinning towards crystal edges) was done taking into account the constant content of oxygen in micrite crystals.

Low-dose illumination conditions were used to study all samples and to record the images. Sufficient statistics in elemental microanalysis can be obtained using long-duration mapping. Therefore Mg mapping up to 10 h was performed by a slightly defocused electron beam to reduce the radiation damage. This defocusing permits the original image of micrite to be preserved because crystals are not damaged, as usually happens with a fully focused beam. In total, 19 highly precise Mg maps of 19 different micrite crystals were obtained on the five different samples (1,405: four maps; 3,816 m: two maps; 3,829 m: five maps; 3,878 m: two maps; 3,897 m: six maps).

Results

Petrophysical, mineralogical, and chemical analyses

The five studied micritic samples (Qatar: 1,405 m; Iraq: 3,816, 3,829, 3,878, 3,897 m) all possess very low Mg content in calcite ($\sim$1% MgO) (Table 1). Two samples are tight (phi $<$ 2.4%, K $<$ 12 mD; Iraq: 3,816, 3,878 m) and three are characterized by a microporous network (11.2% $<$ phi $<$ 19.4%, 79 mD $<$ K $<$ 444 mD; Qatar: 1,405 m; and Iraq: 3,829, 3,897 m) (Table 1).

SEM

Electron channeling contrast formed as a result of backscattering events in a thin layer (sample from Iraq, 3,816 m) was used to obtain a broad visualization of micrite crystals (Figs. 1, 2). The origin of the bright grey and dark grey contrast for different grains is only due to their

Table 1 Depositional texture, bioclastic content, depositional environment, age, petrophysical properties (porosity and permeability), and Mg content for the five studied samples

Country	Well	Depth (m)	Depositional texture	Bioclastic content	Depositional environment	Age	Phi (%)	K (mD)	MgO (%mass)
Qatar	Well Q	1,405	Wackestone	Large foraminifera, rudists, bivalves, echinoderms	Lagoon	Middle to Late Cenomanian	19.4	444	0.14
Iraq	Well X	3,816	Wackestone-packstone	Rudists, bivalves, small foraminifera	Internal platform	Middle to Late Cenomanian	1.1	12	0.95
Iraq	Well X	3,829	Floatstone	Large rudists, bivalves, echinoderms	Internal platform, near rudists-rich shoal	Middle to Late Cenomanian	13.7	324	1.23
Iraq	Well Y	3,878	Wackestone	Rudists, bivalves, echinoderms, small foraminifera	Internal platform	Middle to Late Cenomanian	2.4	4	1.27
Iraq	Well Y	3,897	Wackestone-packstone	Rudists, bivalves, echinoderms	Internal platform	Middle to Late Cenomanian	11.2	79	0.93

different orientation. Their chemical composition within the sensitivity of the microscope is the same.

TEM, STEM, and X-ray EDS

A low magnification STEM image of several dozen micrite crystals (sample from Iraq, 3,816 m) was acquired (Fig. 3a). The same section was afterwards studied by TEM (Fig. 3b). The phase determination performed by analysis of electron diffraction patterns over an area of about 0.5 μm in diameter confirms that micrite crystals are calcite (Fig. 3c).

X-ray EDS microanalyses show that the maximum concentration of Mg in these several dozen micrite crystals previously obtained with STEM (sample from Iraq, 3,816 m) reach 6 at.% in some points (Fig. 4). Heterogeneous distribution of Mg is visible. Some micron size areas have a larger content of Mg than others. However, the compact nature of the sample (phi = 1.1%, K = 12 mD) prevents micrite crystals with well-developed faces from being studied. Thus, for further analyses, only microporous samples (phi > 11%, K > 79 mD) were chosen in order to investigate crystallographic distribution of Mg inside a distinct micrite crystal.

The distribution of Mg inside micrite crystals from microporous samples can be divided into three groups. The first group presents a homogenous concentration of Mg (varying between 0 and 3 at.%) inside a single micrite crystal (Fig. 5a–b, sample from Qatar, 1,405 m). This type

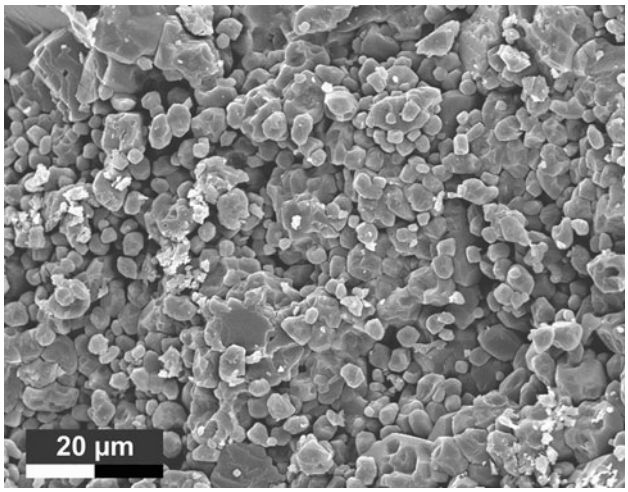

Fig. 1 SEM image of micrite crystals from the Mishrif Formation, a typical microporous carbonate reservoir (sample from Iraq, 3,897 m)

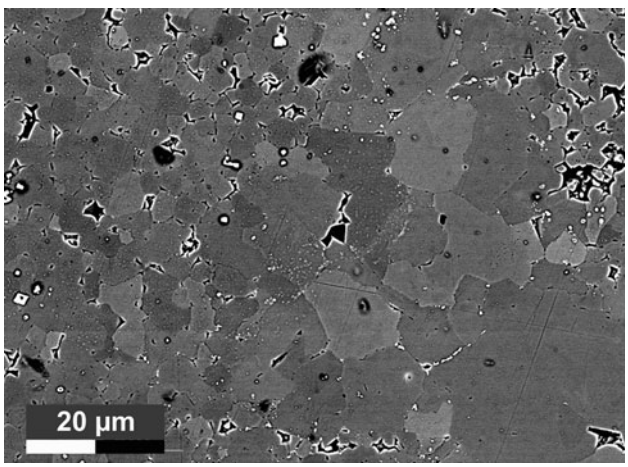

Fig. 2 Backscattered SEM image of micrite crystals (sample from Iraq, 3,816 m) presenting different orientations (*bright to dark grey*) relative to each other. The *black areas* correspond to the microporosity

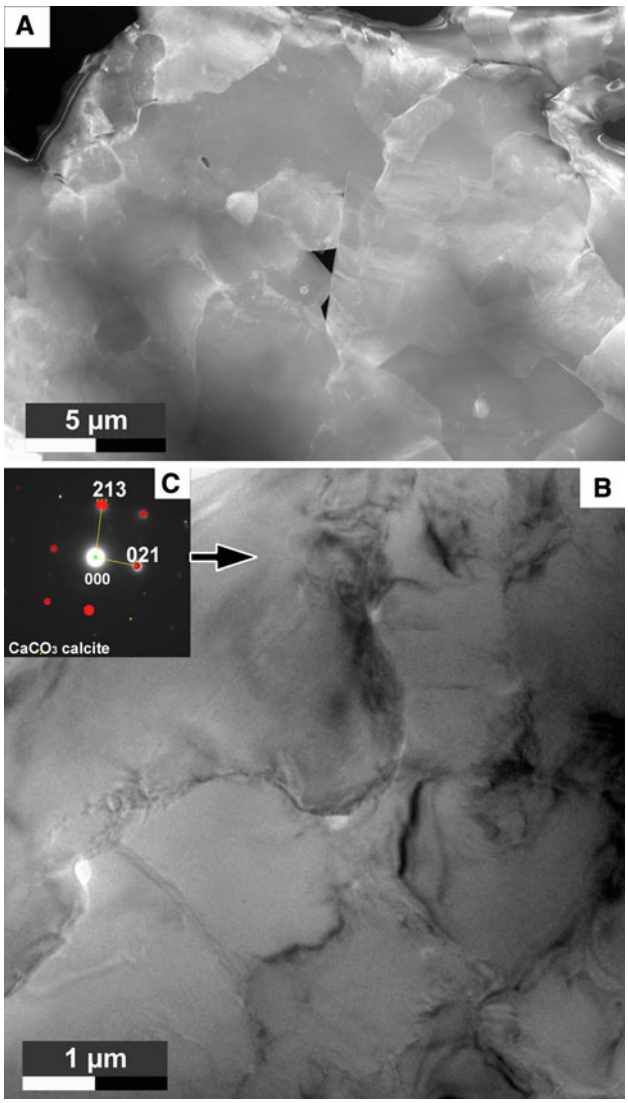

Fig. 3 STEM (**a**) and TEM (**b**) images of micrite crystals (sample from Iraq, 3,816 m). **c** Electron diffraction pattern identifies the mineral phase as calcite (the *arrow* indicates the selected area)

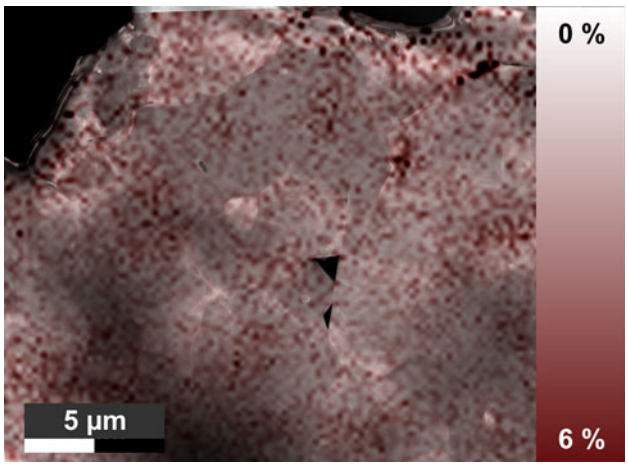

Fig. 4 EDS map of Mg superimposed on STEM image (sample from Iraq, 3,816 m). The intensity of *red* indicates the Mg content

of distribution is the most frequent and was observed in the five different studied samples.

The second group displays Mg-enriched areas far from crystal edges and relatively close to the center (Fig. 5c, d, sample from Iraq, 3,897 m). These enrichments attain about 3 at.%, while the general Mg concentration in the crystal rates about 1–2 at.%. This pattern always comes from micrite crystals of the same sample. Generally, the Mg-enriched areas do not present geometric shapes (Fig. 5c). In one micrite crystal, a rhomboedric shape for the enriched area is evident (Fig. 5d). All of these enrichments cannot be related to thickness changes linked to crystal habits, because of their internal position.

The third group shows geometric impoverishments in Mg near crystal edges (Fig. 5e, f, sample from Iraq, 3,829 m). The Mg concentration in the center of the crystal usually rates about 3–4 at.%, while the borders generally reach less than 1 at.%. Such Mg distribution was always observed in micrite crystals from the same sample. The Mg-poor areas are parallel to present crystallographic faces. However, even taking into account the stoichiometric composition of calcite to correct the thickness effect (thinning towards edges), an artefact for these particular impoverishments cannot be absolutely excluded.

Discussion

Three different types of Mg distribution inside micrite crystals were observed: (1) homogenous, (2) enrichments relatively close to the center of the crystal, and (3) geometric impoverishments near crystal edges and parallel to present crystal faces.

A homogenous distribution of Mg (Fig. 5a, b) is the most frequently encountered and found throughout the five samples. Knowing that micrites from the Mishrif Formation notably underwent meteoric diagenesis linked to the substantial Early Turonian emersion (Alsharhan and Nairn 1993; Haq and Al-Qahtani 2005; Harris et al. 1984), it is surprising not to observe some compositional zonations indicating overgrowths in contact with variable interstitial fluids. One explanation may come from the behavior of Mg towards the calcite in very low Mg/Ca ratio solutions. The incorporation of Mg into calcite is related to the Mg/Ca concentration in solution, but its distribution coefficient increases with decreasing Mg/Ca ratio (Mucci and Morse 1983; Zhong and Mucci 1989). The transition from Cretaceous calcite seawaters to freshwaters induces slight Mg/Ca ratio variations ($\sim$0.5) in the area of very low Mg/Ca ratios (from $\sim$1 to $\sim$0.5). Consequently, the overgrowths precipitated in meteoric interstitial waters may possess very similar Mg concentrations to the more internal parts of the crystal produced from seawater. They may consequently often remain invisible in STEM-EDS Mg maps.

The second type of distribution presents small Mg-enriched areas (<3 at.%) relatively near the crystal center (Fig. 5c, d) that clearly cannot be linked to thickness effects. This particular Mg distribution was always observed in the same sample (Iraq, 3,897). Five of the six micrite crystals analyzed at this level present similar small Mg-enriched areas near the crystal center. This microporous sample (phi = 11.2%, K = 79 mD) is located below (13 m) a substantial emersive surface (unpublished Total report 2009). The small Mg-enriched areas inside micrite crystals may represent seed crystals.

The third type of distribution showing geometric Mg impoverishments near crystal edges and parallel to present faces (Fig. 5e, f) should be interpreted with caution. The Mg-poor zones can either indicate overgrowths with slightly different Mg content, or be the result of a thickness effect linked to crystal thinning towards its edges. However, it is interesting to observe that these Mg-deficient rims were always observed in the same sample (Iraq, 3,829 m). Four of the five micrite crystals investigated at this level show similar geometric Mg impoverishments. The fact that this particular Mg pattern inside micrite crystals was always found in the same sample and was never observed in other ones strongly speaks in favor of a geological origin.

This microporous sample (phi = 13.7%, K = 324 mD) is situated just below (3 m) an important emersive surface (unpublished Total report 2009). In these environmental conditions, Mg-poor zones in the external part of micrite crystals may reflect overgrowths in contact with Mg-poor meteoric waters as the incorporation of Mg into calcite is related to the Mg/Ca concentration in solution (Mucci and Morse 1983; Zhong and Mucci 1989). This result supports the model proposed by Volery et al. (2009, 2010a, b) for

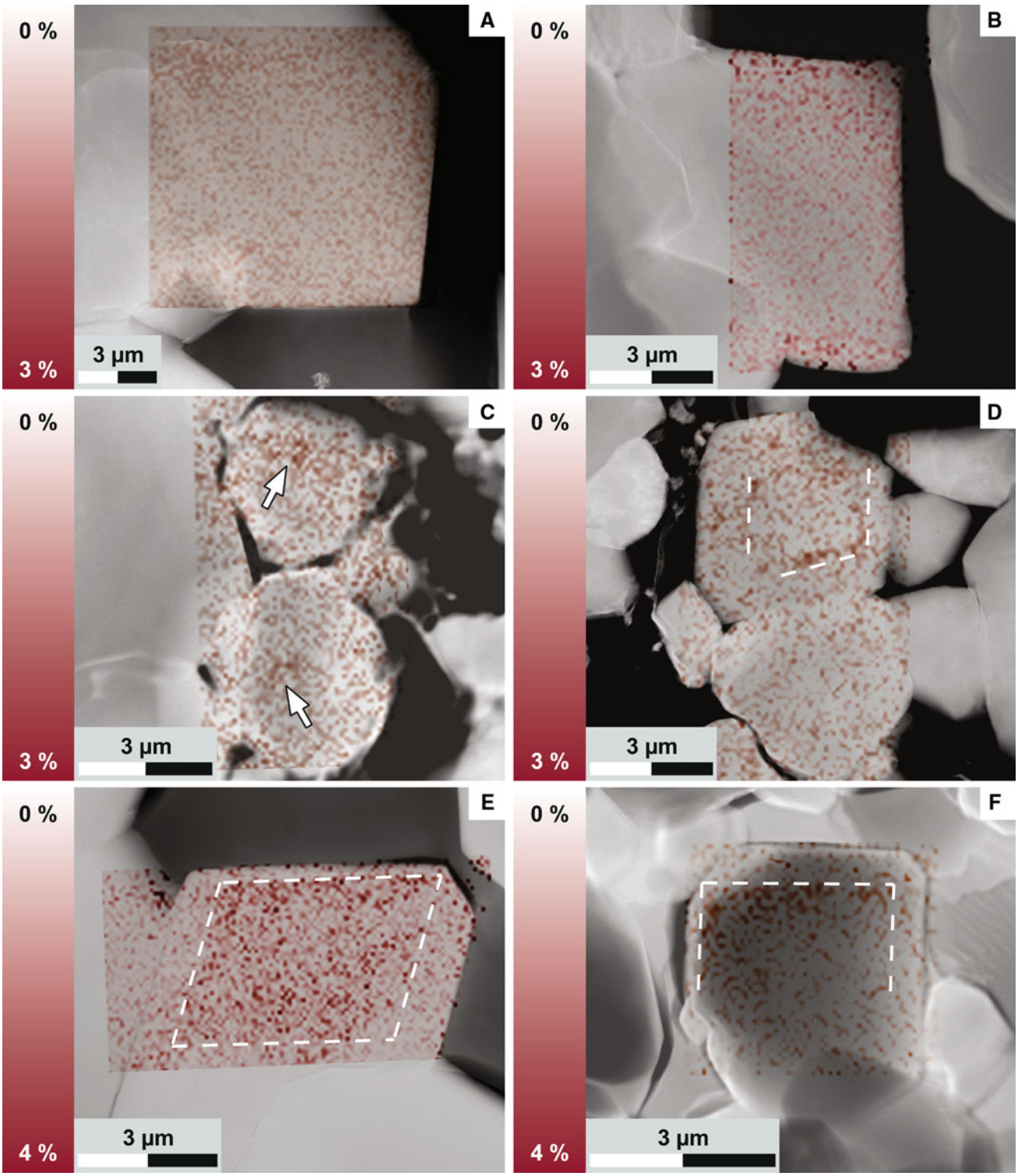

Fig. 5 **a**, **b** EDS maps showing a homogeneous distribution of Mg, within the scale of 0 to 3 at.% (sample from Qatar, 1,405 m). **c**, **d** EDS maps with Mg-enriched areas relatively close to the center of the crystal, within the scale of 0–3 at.% (sample from Iraq, 3,897 m). A rhomboedric shape for the enrichment can be distinguished in image **d**. **e**, **f** EDS maps with geometric Mg impoverishments near crystal edges and parallel to present crystallographic faces, within the scale of 0–4 at.% (sample from Iraq, 3,829 m)

the development and preservation of microporosity in micritic limestones: micrite crystals were originally composed of low-Mg calcite and underwent overgrowths during meteoric diagenesis that lead to the consolidation of their primary microporous framework, which prevents compaction during burial.

This analytical study confronted technical difficulties. The main problem in quantification and interpretation of EDS data combined with STEM comes from radiation damage to the samples. Micrites prepared as ultra-thin sections are very weak under an electron beam. Consequently, maps were recorded under low-dose illuminations and during long-duration mapping. Analyses with more sensitive EDS detectors would reduce the duration of mapping and thus radiation damage. Such technology may improve the signal/noise ratio and precision in the Mg quantification.

Also, a thickness effect cannot be completely excluded even taking into account the stoichiometric composition of $CaCO_3$. The calculations were based on the constant content of oxygen in the crystal; however, this element is very volatile under electron bombardment. Nevertheless, even if precautions should be taken in the interpretations of these maps, notably in the exact value of the Mg content, some recurring patterns of the Mg distribution in micrite crystals observed cannot be only linked to technical artefacts.

Conclusions

This work proposes the first data on the distribution of Mg in micrite crystals obtained with EDS combined with STEM. Through the 19 Mg maps acquired, three types of Mg distribution in micrite crystals were observed. (1) A homogenous Mg concentration (varying between 0 and 3 at.%) is the most frequent distribution. Thus it seems that diagenetic transformations and overgrowths often remain invisible in the behavior of Mg inside micrite crystals. (2) Small Mg-enriched areas (<3 at.%) relatively close to the center of micrite crystals are frequent in micrites of a sample from Iraq (3,829 m) located below an major emersive surface. These enrichments may correspond to crystal seeds. (3) Another sample from Iraq (3,897 m) situated below a substantial emersive surface, shows geometric Mg impoverishments near crystal edges and parallel to present crystallographic faces. An artefact linked to thickness effects cannot be completely excluded. However, because of the limitation of this pattern to only one sample and its persistence throughout different micrite crystals, these Mg-poor borders certainly have a geological signification and may represent overgrowths in contact with less Mg-rich meteoric fluids.

Acknowledgments This research was funded by the University of Geneva and by Total Exploration and Production. The authors would like to thank Robert G. Maliva and John Rejmers for their constructive remarks.

References

Ahr WM (1989) Early diagenetic microporosity in the Cotton Valley Limestone of east Texas. Sediment Geol 63(3–4):275–292

Alsharhan AS, Nairn AEM (1993) Carbonate platform models of Arabian Cretaceous reservoirs. In: Simo JAT, Scott RW, Masse JP (eds) Cretaceous carbonate platforms. AAPG Memoir, vol 56. AAPG, Tulsa, pp 173–184

Aqrawi AAM, Thehni GA, Sherwani GH, Kareem BMA (1998) Mid-Cretaceous rudist-bearing carbonates of the Mishrif Formation: an important reservoir sequence in the Mesopotamian Basin, Iraq. J Pet Geol 21(1):57–82

Budd DA (1989) Micro-rhombic calcite and microporosity in limestones: a geochemical study of the lower Cretaceous Thamama group, U.A.E. Sediment Geol 63(3–4):293–311

Burchette TP (1993) Mishrif formation (Cenomanian-Turonian), Southern Arabian Gulf: carbonate platform growth along a cratonic basin margin. In: Simo JAT, Scott RW, Masse JP (eds) Cretaceous carbonate platforms. AAPG Memoir, vol 56. AAPG, Tulsa, pp 185–199

Cantrell DL, Hagerty RM (1999) Microporosity in Arab formation carbonates, Saudi Arabia. GeoArabia 4(2):129–154

Cavazza W, Roure FM, Spakman W, Stampfli GM, Ziegler PA (2004) The transmed atlas: the Mediterranean region from crust to mantle. Springer, Berlin

Chien YC, Mucci A, Paquette J, Sears SK, Vali H (2006) Comparative study of nanoscale surface structures of calcite microcrystals using FE-SEM, AFM, and TEM. Microsc Microanal 12(4):302–310

Dickson JAD (2002) Fossil echinoderms as monitor of the Mg/Ca ratio of the Phanerozoic oceans. Science 298:1222–1224

Folk RL (1959) Practical petrographic classification of limestones. AAPG Bull 43(1):1–38

Haq BU, Al-Qahtani AM (2005) Phanerozoic cycles of sea-level change on the Arabian platform. GeoArabia 10(2):127–160

Hardie LA (1996) Secular variation in seawater chemistry: an explanation for the coupled secular variation in the mineralogies of marine limestones and potash evaporites over the past 600 m.y. Geology 24(3):279–283

Harris PM, Frost SH, Seiglie GA, Schneidermann N (1984) Regional unconformities and depositional cycles, Cretaceous of the Arabian Peninsula. In: Schlee JS (ed) Interregional unconformities and hydrocarbon accumulation. AAPG Memoir, vol 36. AAPG, Tulsa, pp 67–80

Kaldi J (1989) Diagenetic microporosity (chalky porosity), Middle Devonian Kee scarp reef complex, Norman Wells, Northwest Territories, Canada. Sediment Geol 63(3–4):241–252

Lambert L, Durlet C, Loreau JP, Marnier G (2006) Burial dissolution of micrite in Middle East carbonate reservoirs (Jurassic–Cretaceous): keys for recognition and timing. Mar Pet Geol 23(1):79–92

Loreau JP (1972) Pétrographie de calcaires fins au microscope électronique à balayage: introduction à une classification des "micrites". C R Acad Sci Paris 274(6):810–813

Lowenstein TK, Timofeeff MN, Brennan ST, Hardie LA, Demicco RV (2001) Oscillations in Phanerozoic seawater chemistry: evidence from fluid inclusions. Science 294:1086–1088

Moshier SO (1989) Development of microporosity in a micritic limestone reservoir, Lower Cretaceous, Middle East. Sediment Geol 63(3–4):217–240

Mucci A, Morse JW (1983) The incorporation of Mg^{2+} and Sr^{2+} into calcite overgrowths: influences of growth rate and solution composition. Geochim et Cosmochim Acta 47(2):217–233

Paquette J, Vali H, Mucci A (1996) TEM study of Pt-C replicas of calcite overgrowths precipitated from electrolyte solutions. Geochim et Cosmochim Acta 60(23):4689–4699

Paquette J, Vali H, Mountjoy E (1999) Novel TEM approaches to imaging of microstructures in carbonates; clues to growth mechanisms in calcite and dolomite. Am Mineral 84(11–12): 1939–1949

Perkins RD (1989) Origin of micro-rhombic calcite matrix within Cretaceous reservoir rock, West Stuart City Trend, Texas. Sediment Geol 63(3–4):313–321

Philip J, Borgomano J, Al-Maskiry S (1995) Cenomanian-Early Turonian carbonate platform of northern Oman: stratigraphy and palaeo-environments. Palaeogeogr Palaeoclimatol Palaeoecol 119(1–2):77–92

Pouget EM, Bomans PHH, Goos JACM, Frederik PM, de With G, Sommerdijk NAJM (2009) The initial stages of template-controlled $CaCO_3$ formation revealed by cryo-TEM. Science 323(5920):1455–1458

Reulet J (1977) Réservoir calcaire de plate-forme marine (formation Mishrif, Moyen-Orient)—Carbonate reservoir of a marine shelf: Mishrif Formation (Middle East). In: Elf-Aquitaine (ed) Essai de caractérisation sédimentologique des dépôts carbonatés. Elf-Aquitaine, Boussens-Pau, pp 169–180

Richard J, Sizun JP, Machhour L (2007) Development and compartmentalization of chalky carbonate reservoirs: the Urgonian Jura-Bas Dauphine platform model (Genissiat, southeastern France). Sediment Geol 198(3–4):195–207

Saller AH, Moore CH (1989) Meteoric diagenesis, marine diagenesis, and microporosity in Pleistocene and Oligocene limestones, Enewetak Atoll, Marshall Islands. Sediment Geol 63(3–4):253–272

Sandberg PA (1983) An oscillating trend in Phanerozoic non-skeletal carbonate mineralogy. Nature 305:19–22

Sharland PR, Archer R, Casey DM, Davies RB, Hall SH, Heward AP, Horbury AD, Simmons MD (2001) Arabian Plate sequence stratigraphy. GeoArabia Spec Publ 2. Oriental Press, Manama

Volery C, Davaud E, Foubert A, Caline B (2009) Shallow-marine microporous carbonate reservoir rocks in the Middle East: relationship with seawater Mg/Ca ratio and eustatic sea level. J Petrol Geol 32(4):313–325

Volery C, Davaud E, Foubert A, Caline B (2010a) Lacustrine microporous micrites of the Madrid Basin (Late Miocene, Spain) as analogues for shallow-marine carbonates of the Mishrif reservoir Formation (Cenomanian to Early Turonian, Middle East). Facies 56(3):385–397

Volery C, Davaud E, Durlet C, Clavel B, Charollais J, Caline B (2010b) Microporous and tight limestones in the Urgonian Formation (Late Hauterivian to Early Aptian) of the French Jura Mountains: focus on the factors controlling the formation of microporous facies. Sediment Geol 230:21–34

Zhong S, Mucci A (1989) Calcite and aragonite precipitation from seawater solutions of various salinities: precipitation rates and overgrowth compositions. Chem Geol 78(3–4):283–299

Ziegler MA (2001) Late Permian to Holocene paleofacies evolution of the Arabian Plate and its hydrocarbon occurrences. GeoArabia 6(3):445–504